International Journal of Control, Automation, and Systems 20(10) (2022) 3285-3295
http://dx.doi.org/10.1007/s12555-021-0181-2
ISSN:1598-6446 eISSN:2005-4092
http://www.springer.com/12555

# Robust Finite Time Tracking Control for Robotic Manipulators Based on Nonsingular Fast Terminal Sliding Mode

**Chenchen Sun**

**Abstract:** In this paper, a novel disturbance observer-based robust nonsingular fast terminal sliding mode control (RNFTSMC) technique is proposed for tracking control of robotic manipulators with time-varying disturbances. First, an improved form of nonsingular fast terminal sliding manifold is developed to achieve the strong robustness and finite time convergence of the system, and to avoid the singularity problem. Second, a continuous robust reaching law is designed not only to attenuate chattering phenomena without deteriorating the system tracking precision, but also to guarantee the finite time stability of the system. Furthermore, a nonlinear disturbance observer (NDOB) is employed to estimate the system uncertainties and decrease the switching gain, so that the prior information about the perturbations is not required, and the control signal can be reduced with fewer chattering effect. The system stability is analyzed according to the Lyapunov stability theory. Finally, the superiority of the proposed control scheme is validated by comparative simulation studies.

**Keywords:** Chattering attenuation, nonlinear disturbance observer, nonsingular fast terminal sliding mode control, robotic manipulator, robust reaching law.

## 1. INTRODUCTION

Robotic manipulators have been popularly implemented in industrial fields and hazardous working environments to achieve mechanical automation and ensure safety of operators [1]. They not only have to encounter complex working conditions and various disturbances, but also may confront system uncertainties, such as parameter perturbations and unmodeled dynamics. Moreover, it is difficult to establish comparatively accurate dynamic models for robotic manipulators because of their highly coupled, nonlinear, and time-varying dynamic characteristics [2]. As a result, the control problem of robotic manipulators, especially tracking control, has become a challenging issue and attracted increasing attentions for decades. Advanced control strategies have been proposed to obtain satisfactory tracking performance of robotic systems, such as adaptive control [1,2], feedback linearization [3,4], model predictive control [5], disturbances compensation control [6-8], and sliding mode control (SMC) [9]. Among the existing methods, SMC is under the spotlight owing to its distinguished features on simplified design, invariance to system perturbation, and great robustness against external disturbance. However, the linear switching hyperplane utilized in conventional SMC design only guarantees the asymptotic convergence of the system, and the discontinuous switching control law of SMC leads to unfavorable chattering effect, which may excite high frequency dynamic and result in unexpectable instability.

In recent few decades, the terminal sliding mode control (TSMC) technique utilizing nonlinear switching hyperplanes has been developed to realize the finite time convergence of system states [10-12]. Subsequently, fast terminal sliding mode control (FTSMC) was presented to achieve higher convergence rate and stronger robustness despite large initial system errors [13-15]. However, due to the existence of the negative fractional power, which makes the control input infinite near the equilibrium, conventional TSMC and FTSMC techniques suffer the singularity problem [16-18]. Recently, nonsingular fast terminal sliding mode control (NFTSMC) has been put forward to deal with the singularity issue and perform fast finite time tracking control for practical devices, such as spacecrafts [19], permanent magnet synchronous motors [20], quadrotors [21], and robotic manipulators [22-28]. Besides, integral TSMC technique was another effective means to achieve singularity-free control and ensure the finite time convergence of system tracking errors [29-31].

Chattering is another significant drawback of SMC. To tackle this problem, substantial researches have been proposed over the past few decades. Generally, a saturation function was employed as a substitute for the discontinuous switching function of SMC to reduce chattering

Manuscript received March 1, 2021; revised August 1, 2021 and November 10, 2021; accepted December 14, 2021. Recommended by Associate Editor Maolin Jin under the direction of Editor Kyoung Kwan Ahn. This work is supported by the Key R&D Program of Zhejiang Province [No. 2020C01026].

Chenchen Sun is with the Hangzhou Innovation Institute, Beihang University, Hangzhou 310052, China (e-mail: 11325040@zju.edu.cn).

level [32]. In [27], a smooth function was utilized instead of the discontinuous switching term of NFTSMC to achieve chattering-free control for robotic manipulators. Furthermore, various continuous reaching laws were designed to eliminate chattering. A power reaching law based NTSMC scheme was devised for robotic manipulators to attain high accuracy tracking and alleviate chattering [25]. A global TSMC method adopting a novel fast reaching law was proposed to mitigate chattering and accelerate the convergence rate of the system [33]. An exponential reaching law has been designed for wind turbine systems to obtain desired tracking performance and minimize chattering effect [34,35]. In decades, the second-order SMC technique has been put forward to eliminate chattering phenomena [36,37]. A second-order FTSMC controller was presented to implement high accuracy tracking of uncertain nonlinear systems [38]. An adaptive second-order NTSMC approach was designed for robotic manipulators to achieve favorable tracking performance and chattering attenuation [39]. However, the aforementioned schemes need the prior information about system uncertainties and external disturbances, which is tough to be acquired beforehand in practice. Several studies have integrated adaptive control and disturbance observer techniques into the design of SMC and TSMC to estimate the unknown perturbations [2,12,28,40-42]. Nevertheless, these methods only alleviate chattering level to some extent because the discontinuous control law still exists.

Although numerous control strategies have been presented to address the main issues of robot tracking control, an effective design to deal with the aforementioned problems simultaneously is still challenging. In order to achieve high precision tracking with fewer chattering for robotic manipulators, a novel robust nonsingular fast terminal sliding mode control (RNFTSMC) scheme based on the nonlinear disturbance observer (NDOB) technique is developed in this paper. The main contributions are 1) Unlike the existing works [10-15] that suffer singularity problems, an improved form of nonsingular fast terminal sliding manifold has been utilized to implement fast finite time convergence of the system states and avoid the singularity. 2) Different from the proposed schemes [25,27,32-35] that cannot achieve both high accuracy tracking and chattering reduction, a novel robust reaching law is developed, which can significantly alleviate the chattering effect without reducing the tracking precision and robustness property of the system. 3) The NDOB technique is employed to estimate the uncertainty and disturbance, so that the prior information about system perturbations is unnecessary. Different with the adaptive laws [2,12,28], in which the switching gain should be larger than the upper bound of the perturbation, the adopted NDOB makes the switching gain only need to be greater than the estimation error of the perturbation. Therefore, the proposed controller can further attenuate chattering phenomena and minimize the control signal.

The rest of this paper is structured as follows: The problem is illustrated in Section 2. The proposed RNFTSMC strategy and the system stability analysis are given in Section 3. Section 4 presents the comparative simulations. Conclusions are provided in Section 5.

## 2. PROBLEM FORMULATION

Unlike flexible robots, rigid manipulators can obtain excellent load bearing capacity and high control accuracy without generating undesired vibrations, and their kinetic modes can be established by finite dimensional differential equations [43,44]. In this section, the following $n$ degree of freedom rigid manipulator is considered [22,26]

$$\mathbf{M}(\boldsymbol{\theta})\ddot{\boldsymbol{\theta}}+\mathbf{C}(\boldsymbol{\theta},\dot{\boldsymbol{\theta}})\dot{\boldsymbol{\theta}}+\mathbf{G}(\boldsymbol{\theta})+\mathbf{F}(\boldsymbol{\theta},\dot{\boldsymbol{\theta}})=\boldsymbol{\tau}+\boldsymbol{\tau}_d, \quad (1)$$

where the vector $\boldsymbol{\theta}\in R^n$ denotes the position of the joint; $\mathbf{M}(\boldsymbol{\theta})\in R^{n\times n}$ is a symmetric positive matrix representing the joint inertia; the coriolis force and centrifugal force of the system are expressed by the matrix $\mathbf{C}(\boldsymbol{\theta},\dot{\boldsymbol{\theta}})\in R^{n\times n}$; $\mathbf{G}(\boldsymbol{\theta})\in R^n$ is the gravity vector; $\mathbf{F}(\boldsymbol{\theta},\dot{\boldsymbol{\theta}})\in R^n$ stands for the friction vector; vectors $\boldsymbol{\tau}$ and $\boldsymbol{\tau}_d\in R^n$ denote the control torque of the joint and the external disturbance, respectively. Actually, it is hard to obtain the accurate dynamical models of robotic manipulators in applications. The matrices and vectors in (1) can be represented as

$$\begin{aligned}
&\mathbf{M}(\boldsymbol{\theta})=\mathbf{M_0}(\boldsymbol{\theta})+\Delta\mathbf{M}(\theta),\\
&\mathbf{C}(\boldsymbol{\theta},\dot{\boldsymbol{\theta}})=\mathbf{C_0}(\boldsymbol{\theta},\dot{\boldsymbol{\theta}})+\Delta\mathbf{C}(\boldsymbol{\theta},\dot{\boldsymbol{\theta}}),\\
&\mathbf{G}(\boldsymbol{\theta})=\mathbf{G}_0(\boldsymbol{\theta})+\Delta\mathbf{G}(\boldsymbol{\theta}),
\end{aligned} \quad (2)$$

where $\mathbf{M_0}(\boldsymbol{\theta})$, $\mathbf{C_0}(\boldsymbol{\theta},\dot{\boldsymbol{\theta}})$, and $\mathbf{G}_0(\boldsymbol{\theta})$ are the nominal portion of the system parameters; $\Delta\mathbf{M}(\boldsymbol{\theta})$, $\Delta\mathbf{C}(\boldsymbol{\theta},\dot{\boldsymbol{\theta}})$, and $\Delta\mathbf{G}(\boldsymbol{\theta})$ are the corresponding parameter perturbations.

Consequently, the kinetic model (1) is reformulated as

$$\mathbf{M}_0(\boldsymbol{\theta})\ddot{\boldsymbol{\theta}}+\mathbf{C}_0(\boldsymbol{\theta},\dot{\boldsymbol{\theta}})\dot{\boldsymbol{\theta}}+\mathbf{G}_0(\boldsymbol{\theta})=\boldsymbol{\tau}+\boldsymbol{\Gamma}(\boldsymbol{\theta},\dot{\boldsymbol{\theta}}), \quad (3)$$

where $\boldsymbol{\Gamma}(\boldsymbol{\theta},\dot{\boldsymbol{\theta}})=\boldsymbol{\tau}_d-\Delta\mathbf{M}(\boldsymbol{\theta})\ddot{\boldsymbol{\theta}}-\Delta\mathbf{C}(\boldsymbol{\theta},\dot{\boldsymbol{\theta}})\dot{\boldsymbol{\theta}}-\Delta\mathbf{G}(\boldsymbol{\theta})-\mathbf{F}(\boldsymbol{\theta},\dot{\boldsymbol{\theta}})$ denotes the vector of the bounded lumped uncertainty with $\|\boldsymbol{\Gamma}(\boldsymbol{\theta},\dot{\boldsymbol{\theta}})\|\le D$, and $D$ is a positive constant.

Define the tracking error vector as $\mathbf{e}=\boldsymbol{\theta}-\boldsymbol{\theta}_d=[e_1, e_2, ..., e_n]^T$, where $\boldsymbol{\theta}_d\in R^n$ is the twice differentiable desired position trajectory. This paper aims at designing a robust finite time control scheme to achieve accurate trajectory tracking of robots with system uncertainty and time-varying disturbance.

## 3. THE DESIGN OF RNFTSMC SCHEME BASED ON NDOB

### 3.1. NFTSMC design

For the robotic manipulator (3), the nonsingular fast terminal sliding manifold can be designed as

$$\mathbf{S} = \mathbf{e} + \mathbf{K}_1 \mathrm{diag}(|\mathbf{e}|^{\mathbf{A}})\mathrm{sign}(\mathbf{e}) + \mathbf{K}_2 \mathrm{diag}(|\dot{\mathbf{e}}|^{\mathbf{B}})\mathrm{sign}(\dot{\mathbf{e}}), \tag{4}$$

where $\mathrm{sign}(\cdot)$ is the sign function, $\mathbf{S} = [s_1, ..., s_n]^T$, $\mathbf{K}_1$, $\mathbf{K}_2$, $\mathbf{A}$, and $\mathbf{B}$ are diagonal matrices represented by

$$\begin{aligned}
\mathbf{K}_1 &= \mathrm{diag}(k_{11},\ k_{12},\ ...,\ k_{1n}),\\
\mathbf{K}_2 &= \mathrm{diag}(k_{21},\ k_{22},\ ...,\ k_{2n}),\\
\mathbf{A} &= \mathrm{diag}(\alpha_1,\ \alpha_2,\ ...,\ \alpha_n),\\
\mathbf{B} &= \mathrm{diag}(\beta_1,\ \beta_2,\ ...,\ \beta_n),
\end{aligned}$$

with $k_{1i} > 0$, $k_{2i} > 0$, $1 < \beta_i < 2$, and $\alpha_i > \beta_i$ ($i = 1, 2, ..., n$).

Then, the first derivative of (4) is obtained as

$$\dot{\mathbf{S}} = \dot{\mathbf{e}} + \mathbf{K}_1 \mathbf{A}\mathrm{diag}(|\mathbf{e}|^{\mathbf{A}-\mathbf{I}_n})\dot{\mathbf{e}} + \mathbf{K}_2\mathbf{B}\cdot\mathrm{diag}(|\dot{\mathbf{e}}|^{\mathbf{B}-\mathbf{I}_n})\ddot{\mathbf{e}}, \tag{5}$$

where $\mathbf{I}_n$ is an $n$-dimensional identity matrix.

By solving $\dot{\mathbf{S}} = \mathbf{0}$ on the assumption that $\boldsymbol{\Gamma} = \mathbf{0}$, the equivalent control effort $\boldsymbol{\tau}_{eq}$ is derived as

$$\begin{aligned}
\boldsymbol{\tau}_{eq} = {} & \mathbf{M_0}(\boldsymbol{\theta})\ddot{\boldsymbol{\theta}}_d + \mathbf{C}_0(\boldsymbol{\theta},\dot{\boldsymbol{\theta}})\dot{\boldsymbol{\theta}} + \mathbf{G}_0(\boldsymbol{\theta})\\
& - \mathbf{M}_0(\boldsymbol{\theta})\mathbf{K}_2{}^{-1}\mathbf{B}^{-1}(\mathbf{I}_n + \mathbf{K}_1\mathbf{A}\\
& \times \mathrm{diag}(|\mathbf{e}|^{\mathbf{A}} - \mathbf{I}_n))\mathrm{diag}(|\dot{\mathbf{e}}|^{2\mathbf{I}_n-\mathbf{B}})\mathrm{sign}(\dot{\mathbf{e}}).
\end{aligned} \tag{6}$$

In order to perform expected tracking behaviors in the presence of time-varying perturbations, a discontinuous switching control law is devised as

$$\boldsymbol{\tau}_{sw} = -\mathbf{M_0}(\boldsymbol{\theta})(\mathbf{KS} + \mathbf{H}\mathrm{sign}(\mathbf{S})), \tag{7}$$

where $\mathbf{K} = \mathrm{diag}(k_1,\ k_2,\ ...,\ k_n)$ and $\mathbf{H} = \mathrm{diag}(\eta_1,\ \eta_2,\ ...,\ \eta_n)$ are switching gain matrices with $k_i > 0$ and $\eta_i > 0$.

Therefore, the overall control law of the NFTSMC can be presented as

$$\begin{aligned}
\boldsymbol{\tau} &= \boldsymbol{\tau}_{eq} + \boldsymbol{\tau}_{sw}\\
&= \mathbf{M}_0(\boldsymbol{\theta})\ddot{\boldsymbol{\theta}}_d + \mathbf{C_0}(\boldsymbol{\theta},\dot{\boldsymbol{\theta}})\dot{\boldsymbol{\theta}} + \mathbf{G_0}(\boldsymbol{\theta}) - \mathbf{M_0}(\boldsymbol{\theta})\mathbf{K}_2{}^{-1}\mathbf{B}^{-1}\\
&\quad \times (\mathbf{I}_n + \mathbf{K}_1\mathbf{A}\mathrm{diag}(|\mathbf{e}|^{\mathbf{A}-\mathbf{I}_n}))\mathrm{diag}(|\dot{\mathbf{e}}|^{2\mathbf{I}_n-\mathbf{B}})\mathrm{sign}(\dot{\mathbf{e}})\\
&\quad - \mathbf{M_0}(\boldsymbol{\theta})(\mathbf{KS} + \mathbf{H}\mathrm{sign}(\mathbf{S})).
\end{aligned} \tag{8}$$

To analyze the system stability, the following Lyapunov function is considered

$$V = \frac{1}{2}\|\mathbf{S}\|^2. \tag{9}$$

Differentiating (9) with respect to time and combining (3) yields

$$\begin{aligned}
\dot{V} &= \mathbf{S}^{\mathrm{T}}\dot{\mathbf{S}}\\
&= \mathbf{S}^{\mathrm{T}}(\dot{\mathbf{e}} + \mathbf{K}_1\mathbf{A}\cdot\mathrm{diag}(|\mathbf{e}|^{\mathbf{A}-\mathbf{I}_n})\dot{\mathbf{e}} + \mathbf{K}_2\mathbf{B}\cdot\mathrm{diag}(|\dot{\mathbf{e}}|^{\mathbf{B}-\mathbf{I}_n})\ddot{\mathbf{e}})\\
&= \mathbf{S}^{\mathrm{T}}\begin{bmatrix}
\left(\mathbf{I}_n + \mathbf{K}_1\mathbf{A}\cdot\mathrm{diag}(|\mathbf{e}|^{\mathbf{A}-\mathbf{I}_n})\right)\dot{\mathbf{e}}\\
+ \mathbf{K}_2\mathbf{B}\mathrm{diag}(|\dot{\mathbf{e}}|^{\mathbf{B}-\mathbf{I}_n})\\
\times \left(\mathbf{M_0}^{-1}(\boldsymbol{\theta})\begin{pmatrix}\boldsymbol{\tau} + \boldsymbol{\Gamma}(\boldsymbol{\theta},\dot{\boldsymbol{\theta}})\\ -\mathbf{C}_0(\boldsymbol{\theta},\dot{\boldsymbol{\theta}})\dot{\boldsymbol{\theta}}\\ -\mathbf{G}_0(\boldsymbol{\theta})\end{pmatrix} - \ddot{\boldsymbol{\theta}}_d\right)
\end{bmatrix}\\
&= -\mathbf{S}^{\mathrm{T}}\mathbf{K}_2\mathbf{B}\mathrm{diag}(|\dot{\mathbf{e}}|^{\mathbf{B}-\mathbf{I}_n})\left(\mathbf{KS} + \mathbf{H}\mathrm{sign}(\mathbf{S})\right.\\
&\quad \left. - \mathbf{M_0}^{-1}(\boldsymbol{\theta})\boldsymbol{\Gamma}(\boldsymbol{\theta},\dot{\boldsymbol{\theta}})\right).
\end{aligned} \tag{10}$$

In the absence of parameter perturbation and external disturbance, that is $\boldsymbol{\Gamma} = \mathbf{0}$, (10) is expressed as

$$\begin{aligned}
\dot{V} &= -\mathbf{S}^{\mathrm{T}}\mathbf{K}_2\mathbf{B}\mathrm{diag}(|\dot{\mathbf{e}}|^{\mathbf{B}-\mathbf{I}_n})(\mathbf{KS} + \mathbf{H}\mathrm{sign}(\mathbf{S}))\\
&\le -\min_{i=1,...,n}\left(k_{2i}\beta_i|\dot{e}_i|^{\beta_i-1}k_i\right)\|\mathbf{S}\|^2\\
&\quad -\min_{i=1,...,n}\left(k_{2i}\beta_i|\dot{e}_i|^{\beta_i-1}\eta_i\right)\|\mathbf{S}\|\\
&= -2\min_{i=1,...,n}\left(k_{2i}\beta_i|\dot{e}_i|^{\beta_i-1}k_i\right)V\\
&\quad -\sqrt{2}\min_{i=1,...,n}\left(k_{2i}\beta_i|\dot{e}_i|^{\beta_i-1}\eta_i\right)V^{1/2}\\
&= -\rho_1 V - \rho_2 V^{1/2},
\end{aligned} \tag{11}$$

where $\rho_1 = 2\min_{i=1,...,n}\left(k_{2i}\beta_i|\dot{e}_i|^{\beta_i-1}k_i\right) > 0$ and $\rho_2 = \sqrt{2}\min_{i=1,...,n}\left(k_{2i}\beta_i|\dot{e}_i|^{\beta_i-1}\eta_i\right) > 0$ if $\dot{e}_i \neq 0$. It follows that [28]

$$\begin{aligned}
dt &\le \frac{dV}{-\rho_1 V - \rho_2 V^{1/2}} = \frac{-V^{-1/2}dV}{\rho_1 V^{1/2} + \rho_2}\\
&= \frac{-2dV^{1/2}}{\rho_1 V^{1/2} + \rho_2}.
\end{aligned} \tag{12}$$

Then, integrating (12) from $V(0)$ to $V(t_r)$ yields

$$\begin{aligned}
\int_0^{t_r} dt &\le \int_{V(0)}^{V(t_r)} \frac{-2dV^{1/2}}{\rho_1 V^{1/2} + \rho_2}\\
&= -\frac{2}{\rho_1}\ln\left(\rho_1 V^{1/2} + \rho_2\right)\Big|_{V(0)}^{V(t_r)},
\end{aligned} \tag{13}$$

where $t_r$ is a time constant and $V(t_r) = 0$.

Solving (13), one can obtain

$$t_r \le \frac{2}{\rho_1}\ln\left(\frac{\rho_1 V(0)^{1/2} + \rho_2}{\rho_2}\right). \tag{14}$$

Hence, the sliding manifold $\mathbf{S} = \mathbf{0}$ can be reached within finite time. After that, the system error converges to zero along the manifold in a limited time $T_{nf}$, which is represented as [27]

$$T_{nf} = \int_0^{|e_i(t_r)|} \frac{{k_{2i}}^{1/\beta_i}}{\left(e_i + k_{1i}e_i^{\alpha_i}\right)^{1/\beta_i}} de_i. \tag{15}$$

The preceding analysis is expounded in the case of any $\dot{e}_i \neq 0$, subsequently, the case of $\dot{e}_i = 0$ is to be discussed. Substituting the control effort (8) into (3) yields

$$\ddot{\mathbf{e}} = -\mathbf{K}_2{}^{-1}\mathbf{B}^{-1}(\mathbf{I}_n + \mathbf{K}_1\mathbf{A}\mathrm{diag}(|\mathbf{e}|^{\mathbf{A}-\mathbf{I}_n}))$$

$$\times \operatorname{diag}(|\dot{\mathbf{e}}|^{2\mathbf{I}_n-\mathbf{B}})\operatorname{sign}(\dot{\mathbf{e}}) - (\mathbf{KS}+\mathbf{H}\operatorname{sign}(S)). \quad (16)$$

In the case of $\dot{e}_i = 0$ and $s_i \neq 0$, one can acquire

$$\ddot{e}_i = -k_i s_i - \eta_i \operatorname{sign}(s_i) \neq 0. \quad (17)$$

Therefore, the limited time reachability of the proposed sliding manifold can also be realized.

Consider the system uncertainties, we can obtain

$$\begin{aligned}\dot{V} =& -\mathbf{S}^{\mathrm{T}}\mathbf{K}_2\mathbf{B}\operatorname{diag}(|\dot{\mathbf{e}}|^{\mathbf{B}-\mathbf{I}_n})\begin{pmatrix}\mathbf{KS}+\mathbf{H}\operatorname{sign}(\mathbf{S})\\ -\mathbf{M}_0{}^{-1}(\boldsymbol{\theta})\boldsymbol{\Gamma}(\boldsymbol{\theta},\dot{\boldsymbol{\theta}})\end{pmatrix}\\ \leq& -\min_{i=1,\ldots,n}(k_{2i}\beta_i|\dot{e}_i|^{\beta_i-1}k_i)\|\mathbf{S}\|^2\\ &-\min_{i=1,\ldots,n}(k_{2i}\beta_i|\dot{e}_i|^{\beta_i-1})(\eta_i-\|\mathbf{M}_0{}^{-1}(\boldsymbol{\theta})\|D)\|\mathbf{S}\|\\ =& -2\min_{i=1,\ldots,n}(k_{2i}\beta_i|\dot{e}_i|^{\beta_i-1}k_i)V\\ &-\sqrt{2}\min_{i=1,\ldots,n}(k_{2i}\beta_i|\dot{e}_i|^{\beta_i-1})(\eta_i-\|\mathbf{M}_0{}^{-1}(\boldsymbol{\theta})\|D)V^{1/2}.\end{aligned} \quad (18)$$

According to the foregoing analysis, the finite time stability can be ensured if the switching gain satisfies

$$\eta_{\min} > \left\|\mathbf{M}_0{}^{-1}(\boldsymbol{\theta})\right\| D, \quad (19)$$

where $\eta_{\min} = \min_{i=1,\ldots,n}\eta_i$.

Similar to the argument above, for $\dot{e}_i = 0$ and any $s_i \neq 0$, one can obtain

$$\ddot{e}_i = -k_i s_i - (\eta_i - \Phi_i/\operatorname{sign}(s_i))\operatorname{sign}(s_i) \neq 0, \quad (20)$$

where $\boldsymbol{\Phi} = \mathbf{M}_0{}^{-1}(\boldsymbol{\theta})\boldsymbol{\Gamma}(\boldsymbol{\theta},\dot{\boldsymbol{\theta}}) = (\Phi_1, ..., \Phi_n)^{\mathrm{T}}$.

Hence, the state trajectory can converge to the manifold $\mathbf{S} = \mathbf{0}$ even if $\dot{e}_i = 0$.

**Remark 1:** For the robotic dynamics (3), the conventional terminal sliding manifold is presented as

$$\mathbf{S}_1 = \dot{\mathbf{e}} + \mathbf{K}_3\operatorname{diag}(|\mathbf{e}|^{\mathbf{B}_1})\operatorname{sign}(\mathbf{e}), \quad (21)$$

where $\mathbf{K}_3 = \operatorname{diag}(k_{31}, k_{32}, ..., k_{3n})$, $\mathbf{B}_1 = \operatorname{diag}(\beta_{11}, \beta_{12}, ..., \beta_{1n})$, $k_{3i} > 0$, and $1/2 < \beta_{1i} < 1$ $(i = 1, 2, ..., n)$.

The TSMC control law can be obtained as

$$\begin{aligned}\boldsymbol{\tau}_1 =& \mathbf{M}_0(\boldsymbol{\theta})\ddot{\boldsymbol{\theta}}_d - \mathbf{M}_0(\boldsymbol{\theta})\mathbf{K}_3\mathbf{B}_1\operatorname{diag}(|\mathbf{e}|^{\mathbf{B}_1-\mathbf{I}})\dot{\mathbf{e}}\\ &+\mathbf{C}_0(\boldsymbol{\theta},\dot{\boldsymbol{\theta}})\dot{\boldsymbol{\theta}} + \mathbf{G}_0(\boldsymbol{\theta})\\ &-\mathbf{M}_0(\boldsymbol{\theta})(\mathbf{KS}_1 + \mathbf{H}\operatorname{sign}(\mathbf{S}_1)).\end{aligned} \quad (22)$$

Since $\beta_{1i} - 1 < 0$, $\boldsymbol{\tau}_1$ involves in the singularity issue as the tracking error approaches to the origin, while the adopted NFTSMC can avoid this problem well.

Furthermore, after the manifold $\mathbf{S}_1 = \mathbf{0}$ is arrived, the convergence time of the system error from $e_i(t_r) \neq 0$ to zero can be given as

$$T_t = \int_0^{|e_i(t_r)|}\frac{1}{k_{3i}e_i^{\beta_{1i}}}de_i = \frac{|e_i(t_r)|^{1-\beta_{1i}}}{k_{3i}(1-\beta_{1i})}. \quad (23)$$

Let $\beta_{1i} = 1/\beta_i$ and $k_{3i} = k_{2i}^{-1/\beta_i}$, we can derive

$$\begin{aligned}T_t =& \int_0^{|e_i(t_r)|}\frac{{k_{2i}}^{1/\beta_i}}{e_i^{1/\beta_i}}de_i\\ >& \int_0^{|e_i(t_r)|}\frac{{k_{2i}}^{1/\beta_i}}{(e_i + k_{1i}e_i^{\alpha_i})^{1/\beta_i}}de_i = T_{nf}.\end{aligned} \quad (24)$$

Thus, the convergence rate of the NFTSMC is faster than that of the conventional TSMC.

### 3.2. Robust reaching law design

In general, the saturation function is employed to attenuate chattering phenomena by substituting the discontinuous switching action. The saturation function is defined as

$$\operatorname{sat}(\frac{\mathbf{S}}{\varepsilon}) = \begin{cases}\operatorname{sign}(\mathbf{S}), & \|\mathbf{S}\| > \varepsilon,\\ \mathbf{S}/\varepsilon, & \|\mathbf{S}\| \leq \varepsilon,\end{cases} \quad (25)$$

where $\varepsilon$ is the boundary layer thickness. However, this strategy eliminates chattering at the expense of degenerating the system tracking performance. It can only ensure the finite time convergence of the state trajectory to the thin boundary layer [25].

In order to achieve high accuracy tracking and chattering attenuation, a novel continuous robust reaching law is designed as

$$\begin{aligned}&\dot{\mathbf{S}} = -\mathbf{KS} - \mathbf{H}\operatorname{sat}(\mathbf{S}),\\ &\operatorname{sat}(\mathbf{S}) = \begin{cases}\operatorname{sign}(\mathbf{S}), & \|\mathbf{S}\| > \varepsilon,\\ \dfrac{\mathbf{I}_n - \exp(-\operatorname{diag}(|\mathbf{S}|^{\rho})/\sigma)}{1-\exp(-\varepsilon^{\rho}/\sigma)}\operatorname{sign}(\mathbf{S}), & \|\mathbf{S}\| \leq \varepsilon,\end{cases}\end{aligned} \quad (26)$$

where $\rho > 0$ is an integer, $\sigma > 0$, and $\exp(\cdot)$ represents the exponential function.

Consequently, the robust switching control effort is expressed as

$$\boldsymbol{\tau}_{\mathrm{sw}} = -\mathbf{M}_0(\boldsymbol{\theta})(\mathbf{KS} + \mathbf{H}\operatorname{sat}(\mathbf{S})). \quad (27)$$

Substituting the switching control term in (10) by (27) yields

$$\begin{aligned}\dot{V} =& -\mathbf{S}^{\mathrm{T}}\mathbf{K}_2\mathbf{B}\cdot\operatorname{diag}(|\dot{\mathbf{e}}|^{\mathbf{B}-\mathbf{I}_n})(\mathbf{KS} + \mathbf{H}\operatorname{sat}(\mathbf{S})\\ &-\mathbf{M}_0{}^{-1}(\boldsymbol{\theta})\boldsymbol{\Gamma}(\boldsymbol{\theta},\dot{\boldsymbol{\theta}})).\end{aligned} \quad (28)$$

Similar to the aforementioned stability analysis, when $\|\mathbf{S}\| > \varepsilon$, the state trajectory can tend to the boundary layer in limited time.

When $\|\mathbf{S}\| \leq \varepsilon$, (28) can be represented as

$$\begin{aligned}\dot{V} =& -\mathbf{S}^{\mathrm{T}}\mathbf{K}_2\mathbf{B}\operatorname{diag}(|\dot{\mathbf{e}}|^{\mathbf{B}-\mathbf{I}_n})[\mathbf{KS} + (\mathbf{H}\\ &-\operatorname{diag}(\mathbf{M}_0{}^{-1}(\boldsymbol{\theta})\boldsymbol{\Gamma}(\boldsymbol{\theta},\dot{\boldsymbol{\theta}}))\operatorname{diag}^{-1}(\operatorname{sat}(\mathbf{S})))\operatorname{sat}(\mathbf{S})]\end{aligned}$$

$$
\begin{aligned}
&= -\min_{i=1,\ldots,n}(k_{2i}\beta_i|\dot{e}_i|^{\beta_i-1}k_i)\|\mathbf{S}\|^2 \\
&\quad -\min_{i=1,\ldots,n}(k_{2i}\beta_i|\dot{e}_i|^{\beta_i-1}) \\
&\quad \times\left(\eta_i\frac{1-\exp(-|s_i|^\rho/\sigma)}{1-\exp(-\varepsilon^\rho/\sigma)}-\|\mathbf{M}_0{}^{-1}(\boldsymbol{\theta})\|D\right)\|\mathbf{S}\|.
\end{aligned}
\tag{29}
$$

Obviously, the state trajectory under nominal model ($\boldsymbol{\Gamma}=\mathbf{0}$) can reach the sliding manifold $\mathbf{S}=\mathbf{0}$ within limited time in any cases since $\dot{e}_i=0$ is not an attractor in the reaching stage.

For $\boldsymbol{\Gamma}\neq\mathbf{0}$, the finite time stability condition can be guaranteed if the matrix $\mathbf{H}-\mathrm{diag}(\mathbf{M}_0{}^{-1}(\boldsymbol{\theta})\boldsymbol{\Gamma}(\boldsymbol{\theta},\dot{\boldsymbol{\theta}}))\mathrm{diag}^{-1}(\mathrm{sat}(\mathbf{S}))$ is positive definite, from which one can derive

$$
\eta_{\min}>\frac{\left\|\mathbf{M}_0{}^{-1}(\boldsymbol{\theta})\right\|D(1-\exp(-\varepsilon^\rho/\sigma))}{(1-\exp(-|s_i|^\rho/\sigma))}. \tag{30}
$$

Solving (30) yields

$$
\begin{aligned}
|s_i|>\big[&-\sigma\ln(1-\|\mathbf{M}_0{}^{-1}(\boldsymbol{\theta})\| \\
&\times D(1-\exp(-\varepsilon^\rho/\sigma))/\eta_{\min})\big]^{1/\rho}.
\end{aligned}
\tag{31}
$$

Hence, the following neighborhood of the sliding manifold $\mathbf{S}=\mathbf{0}$ can be reached within limited time

$$
\begin{aligned}
\|\mathbf{S}\|\leq\big[&-\sigma\ln(1-\|\mathbf{M}_0{}^{-1}(\boldsymbol{\theta})\| \\
&\times D(1-\exp(-\varepsilon^\rho/\sigma))/\eta_{\min})\big]^{1/\rho} \\
&<\varepsilon.
\end{aligned}
\tag{32}
$$

Furthermore, (28) can be reformulated into a different form as

$$
\begin{aligned}
\dot{V}=&-\mathbf{S}^{\mathrm{T}}\mathbf{K}_2\mathbf{B}\mathrm{diag}(|\dot{\mathbf{e}}|^{\mathbf{B}-\mathbf{I}_n})\big[(\mathbf{K}-\mathrm{diag}(\mathbf{M}_0{}^{-1}(\boldsymbol{\theta})\boldsymbol{\Gamma}(\boldsymbol{\theta},\dot{\boldsymbol{\theta}})) \\
&\times\mathrm{diag}^{-1}(\mathbf{S}))\mathbf{S}+\mathbf{H}\mathrm{sat}(\mathbf{S})\big].
\end{aligned}
\tag{33}
$$

If the matrix $\mathbf{K}-\mathrm{diag}(\mathbf{M}_0{}^{-1}(\boldsymbol{\theta})\boldsymbol{\Gamma}(\boldsymbol{\theta},\dot{\boldsymbol{\theta}}))\mathrm{diag}^{-1}(\mathbf{S})$ is positive definite, the state trajectory can approach the domain of the manifold $\mathbf{S}=\mathbf{0}$ as

$$
\|\mathbf{S}\|\leq\frac{\|\mathbf{M}_0{}^{-1}(\boldsymbol{\theta})\boldsymbol{\Gamma}(\boldsymbol{\theta},\dot{\boldsymbol{\theta}})\|}{k_{\min}}\leq\frac{\|\mathbf{M}_0{}^{-1}(\boldsymbol{\theta})\|D}{k_{\min}}, \tag{34}
$$

within finite time, where $k_{\min}=\min_{i=1,\ldots,n}k_i$.

In summary, the convergence region of the system trajectory in the presence of perturbations is represented as

$$
\begin{aligned}
&\|\mathbf{S}\|\leq\min(\Omega_1,\Omega_2), \\
&\Omega_1=\frac{\|\mathbf{M}_0{}^{-1}(\boldsymbol{\theta})\|D}{k_{\min}}, \\
&\Omega_2=\big[-\sigma\ln(1-\|\mathbf{M}_0{}^{-1}(\boldsymbol{\theta})\| \\
&\qquad\times D(1-\exp(-\varepsilon^\rho/\sigma))/\eta_{\min})\big]^{1/\rho}.
\end{aligned}
\tag{35}
$$

**Remark 2:** In comparison with the boundary layer approach, the presented robust reaching law can not only improve the tracking precision and robustness of the system, but also effectively attenuate the chattering level.

### 3.3. NDOB design

For the proposed RNFTSMC, the switching gain should be greater than the system perturbations, whose upper bound is hard to be obtained accurately beforehand in practice. Generally, a large enough switching gain is required to guarantee the reachability of the sliding manifold, whereas it will cause a mass of chattering.

In this subsection, a NDOB is employed to compensate the system perturbations and reduce the switching gain, which is designed as [45]

$$
\begin{aligned}
&\dot{\mathbf{z}}=-\boldsymbol{\Lambda}\mathbf{M}_0{}^{-1}(\boldsymbol{\theta})(\boldsymbol{\tau}+\hat{\boldsymbol{\Gamma}}-\mathbf{C}_0(\boldsymbol{\theta},\dot{\boldsymbol{\theta}})\dot{\boldsymbol{\theta}}-\mathbf{G}_0(\boldsymbol{\theta})), \\
&\hat{\boldsymbol{\Gamma}}=\mathbf{z}+\boldsymbol{\Lambda}\dot{\boldsymbol{\theta}},
\end{aligned}
\tag{36}
$$

where $\mathbf{z}$, $\hat{\boldsymbol{\Gamma}}$, and $\boldsymbol{\Lambda}=\mathrm{diag}(\lambda_1,\lambda_2,\ldots,\lambda_n)$ with $\lambda_i>0$ denote the internal state vector of the disturbance observer, the estimation vector of the disturbance, and the observer gain matrix, respectively.

The observation error of $\boldsymbol{\Gamma}$ can be defined as

$$
\tilde{\boldsymbol{\Gamma}}=\boldsymbol{\Gamma}-\hat{\boldsymbol{\Gamma}}. \tag{37}
$$

It is assumed that the observation error is bounded by $\|\widetilde{\boldsymbol{\Gamma}}\|\leq d$, and $d$ is a positive constant.

In practical applications, the disturbances are considered to vary very slowly in every sampling period, namely $\dot{\boldsymbol{\Gamma}}=\mathbf{0}$ [40,45].

Therefore, differentiating (37) yields

$$
\dot{\tilde{\boldsymbol{\Gamma}}}=\dot{\boldsymbol{\Gamma}}-\dot{\hat{\boldsymbol{\Gamma}}}=-\dot{\mathbf{z}}-\boldsymbol{\Lambda}\ddot{\boldsymbol{\theta}}=-\boldsymbol{\Lambda}\mathbf{M}_0{}^{-1}(\boldsymbol{\theta})\tilde{\boldsymbol{\Gamma}}. \tag{38}
$$

Define a Lyapunov candidate function as

$$
V_1=\frac{1}{2}\|\tilde{\boldsymbol{\Gamma}}\|^2. \tag{39}
$$

The first derivative of $V_1$ is presented as

$$
\begin{aligned}
\dot{V}_1&=\tilde{\boldsymbol{\Gamma}}^{\mathrm{T}}\dot{\tilde{\boldsymbol{\Gamma}}}=-\tilde{\boldsymbol{\Gamma}}^{\mathrm{T}}\boldsymbol{\Lambda}\mathbf{M}_0{}^{-1}(\boldsymbol{\theta})\tilde{\boldsymbol{\Gamma}}=-\tilde{\boldsymbol{\Gamma}}^{\mathrm{T}}\boldsymbol{\Xi}\tilde{\boldsymbol{\Gamma}} \\
&\leq-\min_{i=1,\ldots,n}\xi_i\|\tilde{\boldsymbol{\Gamma}}\|^2\leq 0,
\end{aligned}
\tag{40}
$$

where $\boldsymbol{\Xi}=\boldsymbol{\Lambda}\mathbf{M}_0{}^{-1}(\boldsymbol{\theta})=\mathrm{diag}(\xi_1,\ldots,\xi_n)$ with $\xi_i>0$. Evidently, the disturbance observation error can exponentially converge to zero and its convergence rate is determined by the observer gain.

Subsequently, the NDOB based RNFTSMC law is designed as follows, and its block diagram is shown in Fig. 1.

$$
\begin{aligned}
\boldsymbol{\tau}=&\mathbf{M}_0(\boldsymbol{\theta})\ddot{\boldsymbol{\theta}}_{\mathrm{d}}+\mathbf{C}_0(\boldsymbol{\theta},\dot{\boldsymbol{\theta}})\dot{\boldsymbol{\theta}}+\mathbf{G}_0(\boldsymbol{\theta}) \\
&-\mathbf{M}_0(\boldsymbol{\theta})\mathbf{K}_2{}^{-1}\mathbf{B}^{-1}(\mathbf{I}_{\mathrm{n}}+\mathbf{K}_1\mathbf{A}\mathrm{diag}(|\mathbf{e}|^{\mathbf{A}-\mathbf{I}_{\mathrm{n}}})) \\
&\times\mathrm{diag}(|\dot{\mathbf{e}}|^{2\mathbf{I}_{\mathrm{n}}-\mathbf{B}})\mathrm{sign}(\dot{\mathbf{e}})-\mathbf{M}_0(\boldsymbol{\theta})(\mathbf{KS}+\mathbf{H}\mathrm{sat}(\mathbf{S})) \\
&-\hat{\boldsymbol{\Gamma}}.
\end{aligned}
\tag{41}
$$

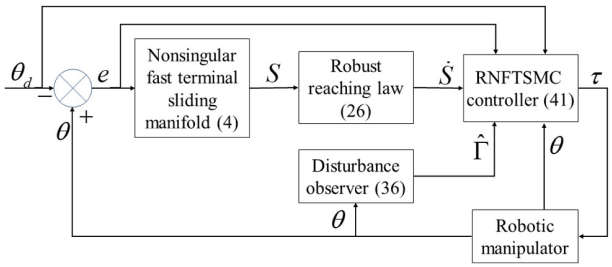


Fig. 1. Structure diagram of the RNFTSMC scheme.

To investigate the stability of the entire closed-loop system, the following Lyapunov function is introduced

$$V_2 = \frac{1}{2}\|\mathbf{S}\|^2 + \frac{1}{2}\|\tilde{\boldsymbol{\Gamma}}\|^2. \tag{42}$$

Differentiating (42) and combining (41) yields

$$\begin{aligned}\dot{V}_2 =& -\mathbf{S}^{\mathrm{T}}\mathbf{K}_2\mathbf{B}\mathrm{diag}(|\dot{\mathbf{e}}|^{\mathbf{B}-\mathbf{I}_n})(\mathbf{K}\mathbf{S}+\mathbf{H}\mathrm{sat}(\mathbf{S}) \\ & -\mathbf{M}_0{}^{-1}(\boldsymbol{\theta})\tilde{\boldsymbol{\Gamma}}) + \tilde{\boldsymbol{\Gamma}}^{\mathrm{T}}\dot{\tilde{\boldsymbol{\Gamma}}} \\ =& \begin{cases} -\mathbf{S}^{\mathrm{T}}\mathbf{K}_2\mathbf{B}\mathrm{diag}(|\dot{\mathbf{e}}|^{\mathbf{B}-\mathbf{I}_n})[\mathbf{K}\mathbf{S}+(\mathbf{H} \\ \quad -\mathrm{diag}(\mathbf{M}_0{}^{-1}(\boldsymbol{\theta})\tilde{\boldsymbol{\Gamma}})\mathrm{diag}^{-1}(\mathrm{sat}(\mathbf{S})))\mathrm{sat}(\mathbf{S})] \\ \quad -\tilde{\boldsymbol{\Gamma}}^{\mathrm{T}}\boldsymbol{\Xi}\tilde{\boldsymbol{\Gamma}}, \\ -\mathbf{S}^{\mathrm{T}}\mathbf{K}_2\mathbf{B}\mathrm{diag}(|\dot{\mathbf{e}}|^{\mathbf{B}-\mathbf{I}_n})[(\mathbf{K}-\mathrm{diag}(\mathbf{M}_0{}^{-1}(\boldsymbol{\theta})\tilde{\boldsymbol{\Gamma}}) \\ \quad \times \mathrm{diag}^{-1}(\mathbf{S}))\mathbf{S}+\mathbf{H}\mathrm{sat}(S)] - \tilde{\boldsymbol{\Gamma}}^{\mathrm{T}}\boldsymbol{\Xi}\tilde{\boldsymbol{\Gamma}}. \end{cases}\end{aligned} \tag{43}$$

According to the aforementioned analysis, the stability condition $\dot{V}_2 \le 0$ can be satisfied if the matrices $\mathbf{H} - \mathrm{diag}(\mathbf{M}_0{}^{-1}(\boldsymbol{\theta})\tilde{\boldsymbol{\Gamma}})\mathrm{diag}^{-1}(\mathrm{sat}(\mathbf{S}))$ and $\mathbf{K} - \mathrm{diag}(\mathbf{M}_0{}^{-1}(\boldsymbol{\theta})\tilde{\boldsymbol{\Gamma}})\mathrm{diag}^{-1}(\mathbf{S})$ are positive definite, from which one can derive

$$\begin{aligned}&\eta_{\min} > |\Sigma_i|, \\ &\eta_{\min} - \frac{|\Sigma_i|(1-\exp(-\varepsilon^{\rho}/\sigma))}{(1-\exp(-|s_i|^{\rho}/\sigma))} > 0, \quad \|\mathbf{S}\| \le \varepsilon, \\ &k_{\min} > |\Sigma_i|/|s_i|,\end{aligned} \tag{44}$$

where $\boldsymbol{\Sigma} = \mathbf{M}_0{}^{-1}(\boldsymbol{\theta})\tilde{\boldsymbol{\Gamma}} = (\Sigma_1, ..., \Sigma_n)^{\mathrm{T}}$.

Consequently, the following convergence domain can be arrived within finite time

$$\begin{aligned}&\|\mathbf{S}\| \le \min(\Omega_1, \Omega_2), \\ &\Omega_1 = \frac{\|\mathbf{M}_0{}^{-1}(\boldsymbol{\theta})\|d}{k_{\min}}, \\ &\Omega_2 = \big[-\sigma\ln(1-\|\mathbf{M}_0{}^{-1}(\boldsymbol{\theta})\| \\ &\qquad \times d(1-\exp(-\varepsilon^{\rho}/\sigma))/\eta_{\min})\big]^{1/\rho}.\end{aligned} \tag{45}$$

Furthermore, the switching gain can be decreased to

$$\eta_{\min} > \|\mathbf{M}_0{}^{-1}(\boldsymbol{\theta})\|d. \tag{46}$$

**Remark 3:** Comparing (46) with (19), the switching gain of the developed composite controller (41) just need to be larger than $\|\mathbf{M}_0{}^{-1}(\boldsymbol{\theta})\|d$ instead of $\|\mathbf{M}_0{}^{-1}(\boldsymbol{\theta})\|D$. Since the lumped uncertainty has been compensated by the NDOB, the upper bound of the observation error is greatly smaller than that of the uncertainty. Hence, the proposed control law can not only enhance the robustness and control performance of the system, but also substantially smooth the control torque and eliminate chattering effect despite large modeling uncertainties and external disturbances.

## 4. SIMULATION RESULTS

In this section, the validity of the adopted NDOB based RNFTSMC controller is investigated on a two degree of freedom robotic manipulator and its superiority is also illustrated by performance comparisons with other advanced methods in [27,28]. The following kinetic model of the manipulator is considered [22,28]

$$\begin{aligned}&\begin{pmatrix} M_{11}(\theta) & M_{12}(\theta) \\ M_{21}(\theta) & M_{22}(\theta) \end{pmatrix}\begin{pmatrix} \ddot{\theta}_1 \\ \ddot{\theta}_2 \end{pmatrix} \\ &+\begin{pmatrix} C_{11}(\theta,\dot{\theta}) & C_{12}(\theta,\dot{\theta}) \\ C_{21}(\theta,\dot{\theta}) & C_{22}(\theta,\dot{\theta}) \end{pmatrix}\begin{pmatrix} \dot{\theta}_1 \\ \dot{\theta}_2 \end{pmatrix} + \begin{pmatrix} G_1(\theta) \\ G_2(\theta) \end{pmatrix} \\ &+\begin{pmatrix} F_1(\theta,\dot{\theta}) \\ F_2(\theta,\dot{\theta}) \end{pmatrix} = \begin{pmatrix} \tau_1 \\ \tau_2 \end{pmatrix},\end{aligned} \tag{47}$$

where

$$\begin{aligned}&M_{11}(\theta) = (m_1+m_2)l_1^2 + m_2l_2^2 + 2m_2l_1l_2\cos(\theta_2) + J_1, \\ &M_{12}(\theta) = M_{21}(\theta) = m_2l_2^2 + m_2l_1l_2\cos(\theta_2), \\ &M_{22}(\theta) = m_2l_2^2 + J_2, \\ &C_{11}(\theta,\dot{\theta}) = -2m_2l_1l_2\sin(\theta_2)\dot{\theta}_2, \\ &C_{12}(\theta,\dot{\theta}) = -m_2l_1l_2\sin(\theta_2)\dot{\theta}_2, \\ &C_{21}(\theta,\dot{\theta}) = m_2l_1l_2\sin(\theta_2)\dot{\theta}_1, \\ &C_{22}(\theta,\dot{\theta}) = 0, \\ &G_1(\theta) = (m_1+m_2)l_1g\cos(\theta_1) + m_2l_2g\cos(\theta_1+\theta_2), \\ &G_2(\theta) = m_2l_2g\cos(\theta_1+\theta_2),\end{aligned}$$

$g = 9.8$ m/s$^2$ is the acceleration of gravity; $m_i$, $l_i$, and $J_i$ ($i = 1, 2$) denote the mass, length, and inertia of the link, respectively. Their nominal values are set to be $m_1 = 0.5$ kg, $m_2 = 1.5$ kg, $l_1 = 1$ m, $l_2 = 0.8$ m, and $J_1 = J_2 = 5$ kg·m$^2$. The initial states of the joint are chosen as $\boldsymbol{\theta}(0) = [0.8,\ 1.5]^T$ and $\dot{\boldsymbol{\theta}}(0) = [-1,\ 1]^T$. Additionally, the reference trajectory is specified as $\boldsymbol{\theta}_d = [1.25 - 1.4e^{-t} + 0.35e^{-4t},\ 1.25 + e^{-t} - 0.25e^{-4t}]^{\mathrm{T}}$.

To make the comparison results fair and convincing, the simulations are implemented under the same conditions. In this work, the fluctuations of system parameters are set as 20% of their nominal values. The friction and the dis-

Table 1. Quantitative analysis.

| Controller | IAE (rad) | | ITAE (rad·s) | |
|---|---|---|---|---|
| | Joint 1 | Joint 2 | Joint 1 | Joint 2 |
| Method in [28] | 0.3237 | 0.4027 | 0.6194 | 2.6276 |
| Method in [27] | 0.2963 | 0.2456 | 0.1511 | 0.2581 |
| RNFTSMC | 0.2952 | 0.2356 | 0.1232 | 0.0959 |

turbance are assumed to be

$$\mathbf{F}(\boldsymbol{\theta},\dot{\boldsymbol{\theta}}) = \begin{pmatrix} F_1(\boldsymbol{\theta},\dot{\boldsymbol{\theta}}) \\ F_2(\boldsymbol{\theta},\dot{\boldsymbol{\theta}}) \end{pmatrix} = \begin{pmatrix} 5\dot{\theta}_1 + 5\text{sign}(\dot{\theta}_1) \\ 5\dot{\theta}_2 + 5\text{sign}(\dot{\theta}_2) \end{pmatrix}, \quad (48)$$

$$\boldsymbol{\tau}_d = \begin{pmatrix} 0.5\sin(200\pi t) + 2\sin(t) \\ 0.5\sin(200\pi t) + \cos(2t) \end{pmatrix}. \quad (49)$$

Moreover, suppose that $m_2$ increases to 3.5 kg when $t \geq 10$ s to simulate sudden load variation.

In order to perform favorable tracking, the coefficients of the proposed NDOB based RNFTSMC are selected as $\mathbf{K}_1 = \text{diag}(1,\ 1)$, $\mathbf{K}_2 = \text{diag}(1,\ 1)$, $\mathbf{A} = \text{diag}(2,\ 2)$, $\mathbf{B} = \text{diag}(5/3,\ 5/3)$, $\mathbf{K} = \text{diag}(100,\ 100)$, $\mathbf{H} = \text{diag}(2,\ 2)$, $\rho = 1$, $\sigma = 0.001$, $\varepsilon = 0.001$, and $\boldsymbol{\Lambda} = \text{diag}(20,\ 20)$ by trial and error method.

The tracking performance comparisons are depicted in Figs. 2-7. It can be figured out from Figs. 2-5 that all the three controllers can make the robot track the reference trajectory accurately before $t = 10$ s. When sudden load variation occurs, the proposed RNFTSMC controller achieves the smallest overshoot and the highest tracking precision, while the method in [28] produces the largest overshoot and tracking errors. Although the method in [27] performs a smooth response, it has small steady state errors. Moreover, as observed in Fig. 6, the RNFTSMC controller and the method in [27] suffer fewer chattering than the method in [28]. It can be found from Fig. 7 that the RNFTSMC controller exhibits the strongest robustness and the fastest convergence rate. Table 1 gives the integral of the absolute value of the error (IAE) and the integral of the time multiplied by the absolute value of the error (ITAE) indices of the three controllers. The two indices are presented by (50) and (51). It is clear that the adopted controller shows lower IAE and ITAE values, and achieves better tracking performance. The results demonstrate that the designed RNFTSMC based on NDOB exhibits superior performance over the existing control strategies, such as more precise tracking, stronger robustness, fewer chattering, and faster response.

$$IAE = \int_0^{t_n} |e_i|\, dt, \quad (50)$$

$$ITAE = \int_0^{t_n} t\,|e_i|\, dt, \quad (51)$$

where $t_n$ is the total running time.

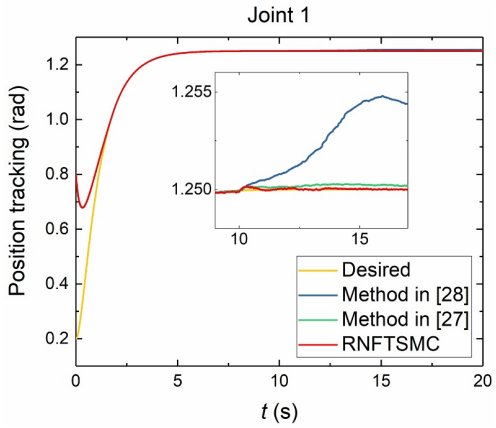


(a) Joint 1.

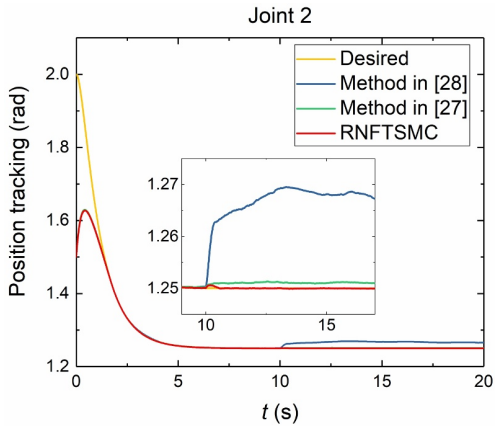


(b) Joint 2.

Fig. 2. Position tracking performance comparisons.

## 5. CONCLUSION

This paper designs a novel RNFTSMC approach based on the NDOB technique for robot tracking under time-varying perturbations. The proposed controller utilizes an improved nonsingular fast terminal sliding manifold to perform finite time convergence and avoid the singularity. Subsequently, a continuous robust reaching law is developed not only to achieve high precision tracking and strong anti-interference ability of the system, but also to attenuate chattering phenomena effectively. Moreover, a NDOB is exploited to compensate system perturbations, so that the prior information about the uncertainties is unnecessary for the design and the control input can be further smoothed. Simulation results indicate the validity and advantages of the presented robust controller by comparative research. In future works, we intend to improve the proposed scheme to remove the reaching stage and achieve global robustness, and evaluate our design on a real robotic system.

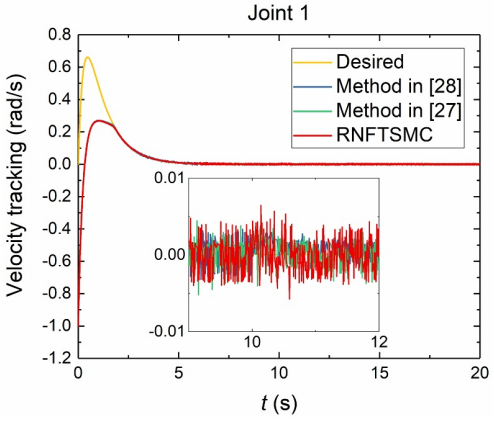


(a) Joint 1.

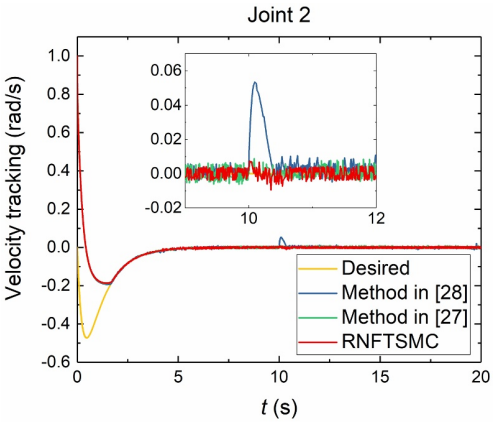


(b) Joint 2.

Fig. 3. Velocity tracking performance comparisons.

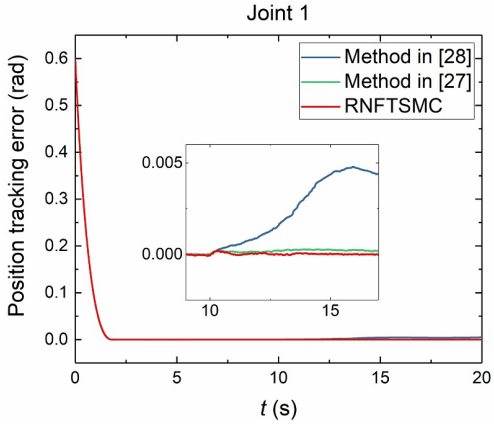


(a) Joint 1.

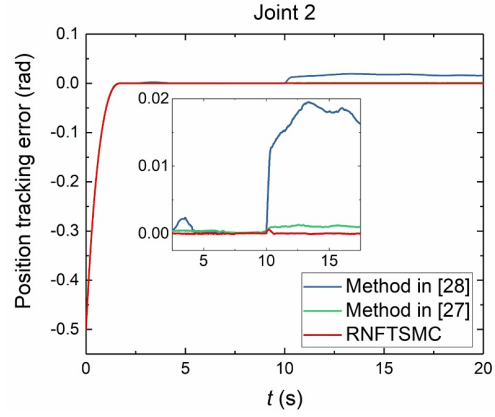


(b) Joint 2.

Fig. 4. Comparisons of position tracking errors.

## REFERENCES


[1] S. Mobayen, F. Tchier, and L. Ragoub, "Design of an adaptive tracker for n-link rigid robotic manipulators based on super-twisting global nonlinear sliding mode control," *International Journal of Systems Science*, vol. 48, no. 9, pp. 1990-2002, 2017.

[2] Q. Cao, S. Li, and D. Zhao, "Adaptive motion/force control of constrained manipulators using a new fast terminal sliding mode," *International Journal of Computer Applications in Technology*, vol. 49, no. 2, pp. 150-156, 2014.

[3] S. Purwar, I. N. Kar, and A. N. Jha, "Adaptive output feedback tracking control of robot manipulators using position measurements only," *Expert Systems with Applications*, vol. 34, no. 4, pp. 2789-2798, 2008.

[4] K. Shojaei, A. M. Shahri, and A. Tarakameh, "Adaptive feedback linearizing control of nonholonomic wheeled mobile robots in presence of parametric and nonparametric uncertainties," *Robotics and Computer-Integrated Manufacturing*, vol. 27, no. 3, pp. 194-204, 2011.

[5] P. Poignet and M. Gautier, "Nonlinear model predictive control of a robot manipulator," *Proc. of the 6th International Workshop on Advanced Motion Control*, pp. 401-406, 2000.

[6] Y. Liu, F. Guo, X. He, and Q. Hui, "Boundary control for an axially moving system with input restriction based on disturbance observers," *IEEE Transactions on Systems, Man and Cybernetics: Systems*, vol. 49, no. 11, pp. 2242-2253, 2019.

[7] Y. Liu, Y. Fu, W. He, and Q. Hui, "Modeling and observer-based vibration control of a flexible spacecraft with external disturbances," *IEEE Transactions on Industrial Electronics*, vol. 66, no. 11, pp. 8648-8658, 2019.

[8] Y. Liu, X. Chen, Y. Wu, H. Cai, and H. Yokoi, "Adaptive neural network control of a flexible spacecraft subject to input nonlinearity and asymmetric output constraint," *IEEE Transactions on Neural Networks and Learning Systems*, pp. 1-9, 2021. DOI: 10.1109/TNNLS.2021.3072907

[9] A. Benamor and H. Messaoud, "Robust adaptive sliding mode control for uncertain systems with unknown time-varying delay input," *ISA Transactions*, vol. 79, pp. 1-12, 2018.

[10] M. Chen, Q. X. Wu, and R. X. Cui, "Terminal sliding mode tracking control for a class of SISO uncertain nonlinear systems," *ISA Transactions*, vol. 52, no. 2, pp. 198-206, 2013.

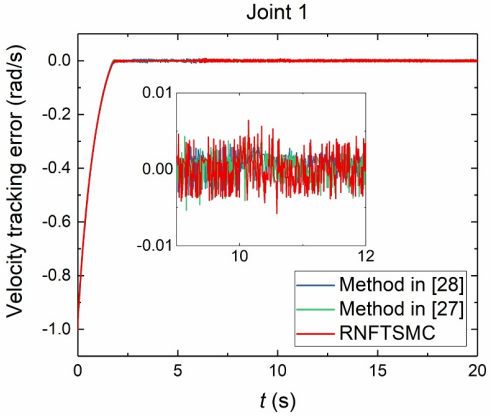


(a) Joint 1.

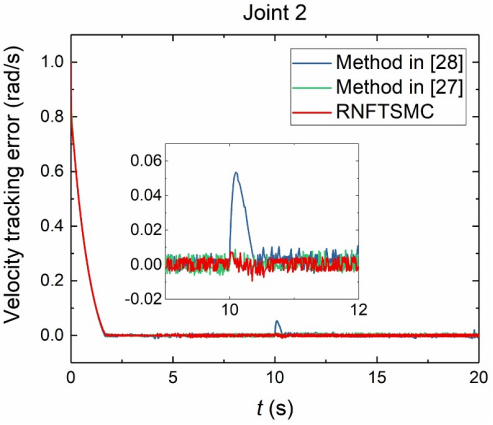


(b) Joint 2.

Fig. 5. Comparisons of velocity tracking errors.

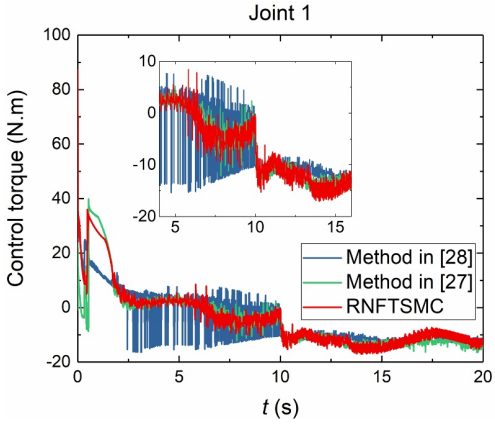


(a) Joint 1.

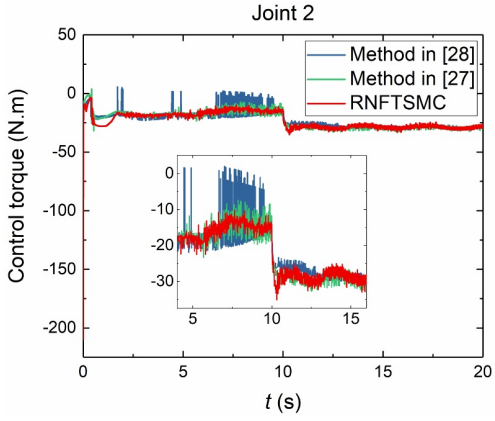


(b) Joint 2.

Fig. 6. Control torque comparisons.

[11] M. L. Jin, S. H. Kang, P. H. Chang, and J. Lee, "Robust control of robot manipulators using inclusive and enhanced time delay control," *IEEE/ASME Transactions on Mechatronics*, vol. 22, no. 5, pp. 2141-2152, 2017.

[12] X. Feng and C. Wang, "Robust adaptive terminal sliding mode control of an omnidirectional mobile robot for aircraft skin inspection," *International Journal of Control, Automation, and Systems*, vol. 19, no. 2, pp. 1078-1088, 2021.

[13] S. Mobayen, "Fast terminal sliding mode controller design for nonlinear second-order systems with time-varying uncertainties," *Complexity*, vol. 21, no. 2, pp. 239-244, 2015.

[14] Q. V. Doan, A. T. Vo, T. D. Le, H. J. Kang, and N. H. A. Nguyen, "A novel fast terminal sliding mode tracking control methodology for robot manipulators," *Applied Sciences*, vol. 10, no. 9, p. 3010, 2020.

[15] K. Eliker and W. Zhang, "Finite-time adaptive integral backstepping fast terminal sliding mode control application on quadrotor UAV," *International Journal of Control, Automation, and Systems*, vol. 18, no. 2, pp. 415-430, 2020.

[16] M. Van, M. Mavrovouniotis, and S. S. Ge, "An adaptive backstepping nonsingular fast terminal sliding mode control for robust fault tolerant control of robot manipulators," *IEEE Transactions on Systems, Man and Cybernetics: Systems*, vol. 49, no. 7, pp. 1448-1458, 2019.

[17] A. T. Vo and H. J. Kang, "A novel fault-tolerant control method for robot manipulators based on non-singular fast terminal sliding mode control and disturbance observer," *IEEE Access*, vol. 8, pp. 109388-109400, 2020.

[18] M. L. Jin, J. Lee, and K. K. Ahn, "Continuous nonsingular terminal sliding-mode control of shape memory alloy actuators using time delay estimation," *IEEE/ASME Transactions on Mechatronics*, vol. 20, no. 2, pp. 899-909, 2015.

[19] C. Pukdeboon and P. Siricharuanun, "Nonsingular terminal sliding mode based finite-time control for spacecraft attitude tracking," *International Journal of Control, Automation, and Systems*, vol. 12, no. 3, pp. 530-540, 2014.

[20] S. Li, M. Zhou, and X. Yu, "Design and implementation of terminal sliding mode control method for PMSM speed regulation system," *IEEE Transactions on Industrial Informatics*, vol. 9, no. 4, pp. 1879-1891, 2013.

[21] G. Zhao, G. Chen, J. Chen, and C. Hua, "Finite-time control for image-based visual servoing of a quadrotor using nonsingular fast terminal sliding mode," *International Journal of Control, Automation, and Systems*, vol. 18, no. 9, pp. 2337-2348, 2020.

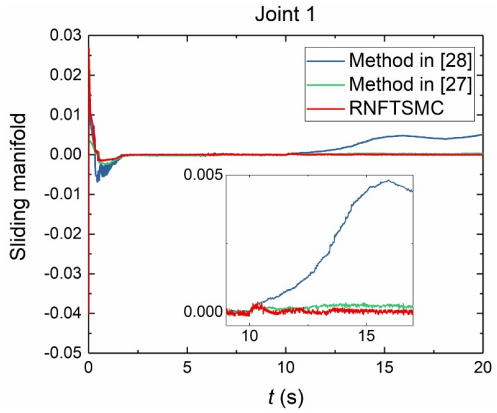


(a) Joint 1.

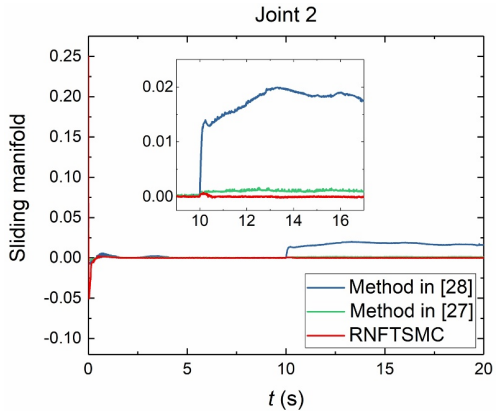


(b) Joint 2.

Fig. 7. Sliding manifold comparisons.


[22] Y. Wang, K. Zhu, B. Chen, and M. Jin, "Model-free continuous nonsingular fast terminal sliding mode control for cable-driven manipulators," *ISA Transactions*, vol. 98, pp. 483-495, 2020.

[23] S. Yi and J. Zhai, "Adaptive second-order fast nonsingular terminal sliding mode control for robotic manipulators," *ISA Transactions*, vol. 90, pp. 41-51, 2019.

[24] V. C. Nguyen, A. T. Vo, and H. J. Kang, "A non-singular fast terminal sliding mode control based on third-order sliding mode observer for a class of second-order uncertain nonlinear systems and its application to robot manipulators," *IEEE Access*, vol. 8, pp. 78109-78120, 2020.

[25] S. Yu, X. Yu, B. Shirinzadeh, and Z. Man, "Continuous finite-time control for robotic manipulators with terminal sliding mode," *Automatica*, vol. 41, no. 11, pp. 1957-1964, 2005.

[26] V. C. Nguyen, A. T. Vo, and H. J. Kang, "A finite-time fault-tolerant control using non-singular fast terminal sliding mode control and third-order sliding mode observer for robotic manipulators," *IEEE Access*, vol. 9, pp. 31225-31235, 2021.

[27] L. Yang and J. Yang, "Nonsingular fast terminal sliding-mode control for nonlinear dynamical systems," *International Journal of Robust and Nonlinear Control*, vol. 21, no. 16, pp. 1865-1879, 2011.

[28] M. Boukattaya, N. Mezghani, and T. Damak, "Adaptive nonsingular fast terminal sliding-mode control for the tracking problem of uncertain dynamical systems," *ISA Transactions*, vol. 77, pp. 1-19, 2018.

[29] J. Lee, M. L. Jin, N. Kashiri, D. G. Caldwell, and N. G. Tsagarakis, "Inversion-free force tracking control of piezoelectric actuators using fast finite-time integral terminal sliding-mode," *Mechatronics*, vol. 57, pp. 39-50, 2019.

[30] S. Mobayen, H. Karami, and A. Fekih, "Adaptive nonsingular integral-type second order terminal sliding mode tracking controller for uncertain nonlinear systems," *International Journal of Control, Automation, and Systems*, vol. 19, no. 4, pp. 1539-1549, 2021.

[31] W. Liu, S. Chen, and H. Huang, "Double closed-loop integral terminal sliding mode for a class of under actuated systems based on sliding mode observer," *International Journal of Control, Automation, and Systems*, vol. 18, no. 2, pp. 339-350, 2020.

[32] F. Cupertino, D. Naso, E. Mininno, and B. Turchiano, "Sliding-mode control with double boundary layer for robust compensation of payload mass and friction in linear motors," *IEEE Transactions on Industry Applications*, vol. 45, no. 5, pp. 1688-1696, 2009.

[33] C. Xiu and P. Guo, "Global terminal sliding mode control with the quick reaching law and its application," *IEEE Access*, vol. 6, pp. 49793-49800, 2018.

[34] Y. Liu, Z. Wang, L. Xiong, J. Wang, X. Jiang, G. Bai, R. Li, and S. Liu, "DFIG wind turbine sliding mode control with exponential reaching law under variable wind speed," *Electrical Power and Energy Systems*, vol. 96, pp. 253-260, 2018.

[35] S. M. Mozayan, M. Saad, H. Vahedi, H. Firtin-Blanchette, and M. Soltani, "Sliding mode control of PMSG wind turbine based on enhanced exponential reaching law," *IEEE Transactions on Industrial Electronics*, vol. 63, no. 10, pp. 6148-6159, 2016.

[36] L. Li, L. Sun, and S. Zhang, "Mean deviation coupling synchronous control for multiple motors via second-order adaptive sliding mode control," *ISA Transactions*, vol. 62, pp. 222-235, 2016.

[37] S. Mobayen and F. Tchier, "A novel adaptive second-order sliding mode tracking control technique for uncertain Dynamical systems with matched and unmatched disturbances," *International Journal of Control, Automation, and Systems*, vol. 15, no. 3, pp. 1097-1106, 2017.

[38] S. Mobayen, D. Baleanu, and F. Tchier, "Second-order fast terminal sliding mode control design based on LMI for a class of non-linear uncertain systems and its application to chaotic systems," *Journal of Vibration and Control*, vol. 23, no. 18, pp. 2912-2925, 2017.

[39] S. Mondal and C. Mahanta, "Adaptive second order terminal sliding mode controller for robotic manipulators," *Journal of The Franklin Institute*, vol. 351, no. 4, pp. 2356-2377, 2014.

[40] J. Yang, S. Li, and X. Yu, "Sliding-mode control for systems with mismatched uncertainties via a disturbance observer," *IEEE Transactions on Industrial Electronics*, vol. 60, no. 1, pp. 160-169, 2013.

[41] X. Shao and H. Wang, "Sliding mode based trajectory linearization control for hypersonic reentry vehicle via extended disturbance observer," *ISA Transactions*, vol. 53, no. 6, pp. 1771-1786, 2014.

[42] Y. Deng, J. Wang, H. Li, J. Liu, and D. Tian, "Adaptive sliding mode current control with sliding mode disturbance observer for PMSM drives," *ISA Transactions*, vol. 88, pp. 113-126, 2019.

[43] Y. Liu, Y. Mei, H. Cai, C. He, T. Liu, and G. Hu, "Asymmetric input-output constraint control of a flexible variable-length rotary crane arm," *IEEE Transactions on Cybernetics*, pp. 1-10, 2021. DOI: 10.1109/TCYB.2021.3055151

[44] Y. Liu, X. Chen, Y. Mei, and Y. Wu, "Observer-based boundary control for an asymmetric output-constrained flexible robotic manipulator," *Science China Information Sciences*, vol. 65, p. 139203, 2022.

[45] A. Mohammadi, M. Tavakoli, H. J. Marquez, and F. Hashemzadeh, "Nonlinear disturbance observer design for robotic manipulators," *Control Engineering Practice*, vol. 21, no. 3, pp. 253-267, 2013.

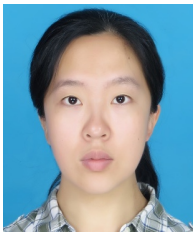

**Chenchen Sun** received her Ph.D. degree in mechatronic engineering from Zhejiang University, Hangzhou, China, in 2020. She is currently working as a postdoctor at Hangzhou Innovation Institute, Beihang University, Hangzhou, China. Her current research interests include automation control, robot control systems, bilateral teleoperation robotic manipulators, and mechatronic systems design.